HHS Public Access

Author manuscript

J Neurosci Res. Author manuscript; available in PMC 2021 September 15.

Published in final edited form as:

J Neurosci Res. 2021 February ; 99(2): 649–661. doi:10.1002/jnr.24737.

Differential Alterations of Insular Cortex Excitability after Adolescent or Adult Chronic Intermittent Ethanol Administration in Male Rats

Yi-Xiao Luo[1,2,*], **Ewa Galaj**[2,*], **Yao-Ying Ma**[1,2,3]

[1]Department of Pharmacology and Toxicology, Indiana University School of Medicine, Indianapolis, IN 46202, USA.

[2]Department of Psychology, Behavioral Neuroscience Program, State University of New York, Binghamton, New York 13902, USA.

[3]Stark Neurosciences Research Institute, Indiana University School of Medicine, Indianapolis, IN 46202, USA.

Abstract

Adolescent alcohol-drinking, primarily in the form of binge-drinking episodes, is a serious public health concern. Binge drinking in laboratory animals has been modeled by a procedure involving chronic intermittent ethanol (CIE) administration, as compared with chronic intermittent water (CIW). The prolonged effects of adolescent binge alcohol exposure in adults, such as high-risk of developing alcohol use disorder, are severe but available treatments in the clinic are limited. One reason is the lack of sufficient understanding about the associated neuronal alterations. The involvement of the insular cortex (IC), particularly the anterior agranular insula (AAI), has emerged as a critical region to explain neuronal mechanisms of substance abuse. This study was designed to evaluate the functional output of the AAI by measuring the intrinsic excitability of pyramidal neurons from male rats 2 or 21 days after adolescent or adult CIE treatment. Decreases of intrinsic excitability in AAI pyramidal neurons were detected 21 days, relative to 2 days, after adolescent CIE. Interestingly, the decreased intrinsic excitability in the AAI pyramidal neurons was observed 2 days after adult CIE, compared to adult CIW, but no difference was found between 2 vs. 21 days after adult CIE. These data indicate that, although the AAI is influenced within a limited period after adult but not adolescent CIE, neuronal alterations of AAI are affected during the prolonged period of withdrawal from adolescent but not adult CIE. This may explain the prolonged vulnerability to mental disorders of subjects with an alcohol binge history during their adolescent stage.

CORRESPONDING AUTHOR: Dr. Yao-Ying Ma, Department of Pharmacology and Toxicology, Indiana University School of Medicine, 635 Barnhill Drive, Indianapolis, IN 46202, Tel: 317-274-1536 Fax: 317-274-7714, ym9@iu.edu.

*YX Liu and E Galaj contributed equally to this work.

Author Contributions

YL and YM were responsible for experimental design. YL and EG were responsible for data collection. YL, EG and YM were responsible for data analysis and paper drafting.

CONFLICT OF INTEREST STATEMENT: The authors report no conflicts of interest.

DISCLOSURE

The authors report no conflicts of interest.

Keywords

Chronic Intermittent Ethanol; Adolescent; Insular Cortex; Intrinsic Excitability; Whole-cell patch clamp

INTRODUCTION

Alcohol is the most widely used substance of abuse, and most people in the United States begin to use alcohol during adolescence (National Institute on Alcohol Abuse and Alcoholism, 2017; Spear & Swartzwelder, 2014). Adolescent alcohol-drinking is a serious public health concern, with 7.7 million individuals between the ages of 12–20 years reporting drinking alcohol within the past month (Substance Abuse and Mental Health Services Administration, 2015). In particular, at least one binge-drinking episode in the past month was reported by 5.1 million underage drinkers and over 90% of alcohol consumed by underage drinkers was in the form of binge-drinking episodes (National Institute on Alcohol Abuse and Alcoholism, 2017). This high prevalence of binge alcohol drinking occurs at a critical period during development when the central nervous system is undergoing rapid adaptations in structure and function that could lead to subsequent susceptibility to mental disorders. The behavioral consequences, especially the prolonged effects of adolescent alcohol exposure in the clinic (e.g., high-risk of developing alcohol use disorder) cause substantial morbidity, but available treatments are limited (Kyzar, Zhang, & Pandey, 2019; Sakharkar et al., 2019; Viner & Taylor, 2007). One reason is the lack of sufficient understanding about the neuronal alterations induced by adolescent binge alcohol exposure, and how these changes contribute to the increased risk of alcohol abuse, even after a prolonged withdrawal period. Binge drinking in laboratory animals has been modeled by chronic intermittent ethanol (CIE) administration, which could help in our understanding of potential mechanisms.

The role of the cerebral cortex in mediating substance abuse-related behaviors has mainly focused on the medial prefrontal cortex (Abernathy, Chandler, & Woodward, 2010; Klenowski, 2018; Park et al., 2010; Trantham-Davidson et al., 2014). However, in the past two decades, the involvement of the insular cortex (IC), or insula for short, emerged as a key element in neuronal mechanisms of substance abuse. A great variety of functions of the IC have been identified, ranging from sensory processing to representation of feelings and emotions, autonomic and motor control, risk prediction and decision-making, body- and self-awareness, and complex social functions like empathy (Gogolla, 2017). Both human (Damasio et al., 2000; Franklin et al., 2002; Naqvi, Rudrauf, Damasio, & Bechara, 2007) and animal studies (Contreras, Ceric, & Torrealba, 2007) showed that IC lesions interrupt addictive behaviors, suggesting that the IC or the IC-mediated interoceptive system is sensitized in vulnerable subjects as a consequence of addiction history and a cause of relapse. However, an opposite picture was depicted by neuroimaging studies, in which reduced activity (Stewart, Connolly, et al., 2014; Stewart, May, et al., 2014) and shrunken gray matter (Franklin et al., 2002; Mackey & Paulus, 2013) in the IC was detected in individuals with substance abuse history. These apparently contradictory lines of evidence may indicate that the IC can both promote substance abuse (e.g., via increased perception

of craving for drugs) or weaken the processes that prevent substance abuse, such as decision-making and the evaluation of negative consequences (Gogolla, 2017). Although the precise role played by the IC in alcohol abuse-related behavior remains unknown, it has been established that IC dysfunction underlies substance abuse and mechanistic studies on the insula is a potential way to answer this question.

The IC, as part of the cerebral cortex, lies deep within the temporal lobe in primates, including humans, and surrounds the rhinal fissure in rodents. It consists of 3 sub-regions (i.e., posterior granular insular, anterior agranular insula (AAI), and the intermediate dysgranular insula) across species (Allen, Saper, Hurley, & Cechetto, 1991; Teofilovski, 1984; Uddin, Nomi, Hebert-Seropian, Ghaziri, & Boucher, 2017). Particular attention in addiction research has been paid to the AAI due to its rich chemoarchitecture (Naqvi et al., 2007). First, The AAI receives dense dopaminergic innervation (Gaspar, Berger, Febvret, Vigny, & Henry, 1989), contains a high density of D1 dopamine receptors (Hurd, Suzuki, & Sedvall, 2001), and both D1 and D2 receptors in the AAI are engaged in behavioral output control (Suhara et al., 2001). Second, both endogenous opioids (Evans, Bey, Burkey, & Commons, 2007) and the mu-opioid receptors (Baumgartner et al., 2006; Burkey, Carstens, Wenniger, Tang, & Jasmin, 1996) were detected in the AAI at a high density, indicating the involvement of AAI in pain modulation and mu opioid receptor-related emotion, motivation and addiction behaviors. Third, type 1 corticotrophin-releasing hormone receptors, which might mediate stress-triggered alcohol intake (Shillinglaw, Morrisett, & Mangieri, 2018), was reported at a high density in the AAI. Thus, the current study was designed to unravel the effects of CIE exposure on the excitability or functional output of AAI pyramidal neurons.

The functional output of a brain region, by definition, is the action potential of the projecting neurons in that region (Hille, 2001), which is directly associated with the intrinsic excitability of these neurons (Ma et al., 2012). However, it is unclear how the intrinsic membrane excitability of the projecting pyramidal neurons in the AAI is affected by CIE treatment, especially after a prolonged withdrawal period (21 days in the present study) after *adolescent CIE* (also denoted AIE in the literature, standing for adolescent intermittent ethanol). CIE, as well as chronic intermittent water (CIW) as control, was administered to adolescent (postnatal (P) day 28–46 and adult (P70–88) Sprague Dawley rats, to mimic adolescent and adult alcohol binge exposure in humans. The intrinsic excitability of projection pyramidal neurons in the AAI was measured both 2 days and 21 days after the last gavage intubation by whole-cell patch clamp recordings. Relative to that in CIW-treated controls, decreased intrinsic excitability in AAI pyramidal neurons was detected 2 days after adult CIE treatment, relative to 2 days after adult CIE treatment. However, adolescent CIE decreased the AAI excitability on withdrawal day (WD) 21, compared to WD 21 after adolescent CIE treatment. We conclude that active alterations in the AAI region occur during the withdrawal period after adolescent CIE, but only transient changes in the AAI after adult CIE. This indicates a prolonged mental risk of subjects with an alcohol binge history during their adolescent stage.

MATERIALS AND METHODS

Experimental Subjects:

All procedures were performed in accordance with the United States Public Health Service Guide for Care and Use of Laboratory Animals and were approved by the Institutional Animal Care and Use committee at Indiana University School of Medicine and the State University of New York, Binghamton. Experiments were conducted on 41 male Sprague-Dawley rats, bred in-house using breeders originally derived from Envigo, USA, and randomly assigned to different groups. With the day of birth being deemed as P0, rats were weaned at P21–23 and pair-housed in standard Plexiglas cages with shredded paper as environmental enrichment. Rats were maintained on a 7 AM / 7 PM light / dark schedule with ad libitum access to food and water under controlled temperature (22 ± 2 °C) and humidity (50 ± 15%). Cages were changed weekly. Rats were handled to habituate them to human contact prior to experimentation.

Chronic intermittent ethanol exposure:

Our CIE procedure was described in our recent publication (Shan, Galaj, & Ma, 2019). Briefly, adolescent (“Ado”, P28-P47 or adult “Adu”, P70-P89) rats received 4.0 g/kg intragastric (IG) administration of 25% (v/v) ethanol (CIE) or equivalent volume of water (CIW) once per day at approximately 9:00 AM in a 3-day on and 2-day off pattern as one cycle, repeated 4 times in total. Blood ethanol concentrations were assessed via headspace gas chromatography using a Hewlett Packard (HP) 5890 series II Gas Chromatograph (Wilmington, DE). Our data show that, Ado::CIE and Adu::CIE resulted in similar increases of BECs by the end of cycle 2 (in mg/dL: Ado::CIW, 13.5±0.6; Adu::CIW, 12.2±0.5; Ado::CIE, 170.2±9.1; Adu::CIE, 166.3±12.3; two-way ANOVA showed Ado/Adu × CIW/CIE interaction $F_{1,20}$=0.7, p=0.31, Ado/Adu $F_{1,20}$=1.7, p=0.20, although CIW/CIE $F_{1,20}$=43.2, p<0.01) and cycle 4 (in mg/dL: Ado::CIW, 11.1±0.9; Adu::CIW, 11.2±0.9; Ado::CIE, 194.7±13.1; Adu::CIE, 184.1±11.4; two-way ANOVA showed Ado/Adu × CIW/CIE interaction $F_{1,20}$=0.8, p=0.37, Ado/Adu $F_{1,20}$=1.5, p=0.24, although CIW/CIE $F_{1,20}$=41.0, p<0.01), similar to our previous publication (Shan et al., 2019). These concentrations are in the binge range (defined as >80 mg/dL by the NIAAA). In addition, more details about the experimental procedure are available in Fig. 1A.

Brain slice whole-cell patch clamp recordings:

Standard procedures were used for preparing slices and whole-cell patch clamp recordings as detailed in our previous publications (Ma et al., 2012; Ma et al., 2014; Ma et al., 2016). Before sacrifice, the rats were anesthetized with isoflurane and subsequently transcardially perfused with 4°C cutting solution (in mM: 135 *N*-methyl-D-glucamine, 1 KCl, 1.2 KH_2PO_4, 0.5 $CaCl_2$, 1.5 $MgCl_2$, 20 choline-HCO_3, 11 glucose, pH adjusted to 7.4 with HCl, and saturated with 95% O_2 /5% CO_2). The rat was decapitated, and then the brain was removed and glued to a block before slicing using a Leica VT1200s vibratome in 4°C cutting solution. Coronal slices of 250 μm thickness were cut such that the preparation contained the signature anatomical landmarks (e.g., the rhinal fissure, the anterior commissure and the corpus callosum as shown in Fig. 1B) that clearly delineate the AAI area. After allowing at least 1 hr for recovery, slices were transferred from a

holding chamber to a submerged recording chamber where it was continuously perfused with oxygenated ACSF maintained at 30 ± 1°C. The pyramidal neurons in the AAI were visualized (Fig. 1C) by Retiga ELECTRO CCD camera (Teledyne Photometrics) mounted on an Olympus BX51WI microscope.

Standard whole-cell current- or voltage-clamp recordings were obtained with a MultiClamp 700B amplifier (Molecular Devices), filtered at 3 kHz, amplified 5 times, and then digitized at 20 kHz with a Digidata 1550B analog-to-digital converter (Molecular Devices). The recording electrodes (3–5 MΩ) were filled with (in mM): 108 $KMeSO_3$, 20 KCl, 0.4 K-EGTA, 10 Hepes, 2.5 Mg-ATP, 0.25 Na-GTP, 7.5 phosphocreatine (2Na), 1 L-glutathione, 2 $MgCl_2$, pH 7.3. The recording bath solution contained (in mM): 119 NaCl, 2.5 KCl, 2.5 $CaCl_2$, 1.3 $MgCl_2$, 1 NaH_2PO_4, 26.2 $NaHCO_3$, and 11 glucose, saturated with 95% O_2 / 5% CO_2 at 30 ± 1°C. Details for whole-cell patch clamp recordings can be found in one of our previous publications (Ma et al., 2012). Cells were patched in voltage clamp mode and held at −70 mV. Cell membrane capacitance (Cm), input resistance (Rm) and time constant (τ) were calculated by applying a depolarizing step voltage command (5 mV) and using the membrane test function integrated in the pClamp11 software. Then recordings were switched to current clamp mode. Resting membrane potential (RMP) was adjusted to −70± 0.05 mV via injection of positive current (50 – 100 pA) and then intrinsic excitability was examined using a series of depolarizing current pulses and constructing input-output (I-O) functions.

Morphological confirmation of insular pyramidal neurons:

Brain slices containing biocytin-filled cells were fixed with 4% paraformaldehyde in 0.1 M phosphate buffer, pH 7.4, for 2 h. Slices were washed three times for 5, 10 and 60 min respectively in 0.05 M TBST (TBS containing 0.1% Tween 20). Then they were incubated at 4°C overnight with Alexa Fluor® 488-conjugated streptavidin (Invitrogen; dilution 1:1000 with TBST) and washed with TBST. Images were obtained with a confocal laser scanning microscope (SP2 1P-FCS, Leica). An example staining is shown in Fig. 1D.

Data Acquisition and Analysis

Data were collected either 2 days or 21 days after the last intubation of water or ethanol, and processed blindly whenever allowed. All results are shown as mean ± SEM. Recordings were replicated on 2–4 cells per rat from no less than 4 rats per group. AAI pyramidal neurons, similar to other cerebral regions, have typical spiking patterns (as shown in Figs. 2, 4), and morphologically have a triangle-shaped soma (Φ=15-μm), with spiny basal and apical dendrites and a non-spiny axon. Those showing either atypical electrophysiological properties (e.g., different spiking patterns, outliers in terms of basic membrane properties, i.e., Cm, Rm, τ, and RMP), and / or atypical morphology based on biocytin imaging were excluded. Sample size is presented as m/n, where “m” refers to the number of cells examined and “n” refers to the number of rats. Statistical significance was assessed using two-way ANOVA (summarized results in Figs. 3B,G–I; 5B,G–I; 8A,B) or two-way ANOVA with repeated measures (summarized results in Figs. 2C–F; 3C–F; 4C–F; 5C–F; 6A–D; 7A–D), followed by Bonferroni post-hoc tests. Data in Figs. 2–8 were also analyzed by three-way ANOVA and/or nested t test. See more details in figure legends. Data were

analyzed both by cell-based and animal-based ways (i.e., values from multiple cells of one animal were averaged to represent this animal). More importantly, nested analyses were performed on the data supporting our key conclusions. This analysis combines the power from both the number of animals and the number of cells per animal (Figs. 2D, 3D, 4E, 5E).

RESULTS

Different effects of adolescent *vs*. adult CIE on IC excitability

Decreased excitability 21 days but not 2 days after CIE during adolescent stage—Electrophysiological studies in IC-containing coronal slices from rats treated by CIW/CIE during their adolescent stage were performed 2 days or 21 days after the last intubation to administer ethanol. Whole-cell patch clamp recordings of pyramidal neurons in the IC (example traces in Fig. 2A&B) from Ado::CIE rats showed a voltage-dependent decrease of spike number on WD21, relative to WD2 (Fig. 2D, I_{inj} × WD2/WD21 interaction $F_{10,290}$=9.9, p<0.01, cell-based; I_{inj} × WD2/WD21 interaction $F_{10,70}$=4.6, p<0.01, animal-based). However, no significant differences of spike number on WD2 *vs*. WD21 were detected on Ado::CIW rats (Fig. 2C, I_{inj} × WD2/WD21 interaction $F_{10,300}$=1.3, p=0.21, cell-based; I_{inj} × WD2/WD21 interaction $F_{10,80}$=1.6, p=0.12, animal-based). Interestingly, no differences of spike numbers between Ado::CIW *vs*. Ado::CIE were detected in rats both 2 days (Fig. 2E, I_{inj} × CIW/CIE interaction $F_{10,300}$=0.7, p=0.68, cell-based; I_{inj} × CIW/CIE interaction $F_{10,70}$=0.6, p=0.79, animal-based) and 21 days (Fig. 2F, I_{inj} × CIW/CIE interaction $F_{10,290}$=0.6, p=0.77, cell-based; I_{inj} × CIW/CIE interaction $F_{10,80}$=0.7, p=0.72, animal-based) after the adolescent treatment. Nested t test on the spike number at I_{inj}=600pA in **D** showed a significant decrease on WD21, relative to that on WD2 after Ado::CIE (t_{29}=3.6, p<0.01). Further three-way ANOVA analyses on the spike number from both Ado::CIW and Ado::CIE on WD2 and WD21 (i.e., the data from both **C** and **D**, or from both **E** and **F**) showed a significant interaction of WD2/WD21 × Ado::CIW/Ado::CIE ($F_{1,59}$=4.1, p=0.046), although no significance on I_{inj} × WD2/WD21 × Ado::CIW/Ado::CIE interaction $F_{10,590}$=1.2, p=0.30. Thus, Ado::CIE-induced changes in IC excitability were withdrawal stage-dependent. Specifically, the decrease in IC excitability took time to be fully expressed after Ado::CIE.

Delayed after-fAHP depolarization 21 days after adolescent CIE treatment —Neuronal intrinsic excitability is tightly regulated by the amplitude of the afterhyperpolarization (AHP) (example traces in Fig. 3A) and its depolarization. It has been shown that decreased amplitude of AHP leads to an increase in excitability (Honrath, Krabbendam, Culmsee, & Dolga, 2017). Further data analyses on the 2nd spike as a response induced by 300 ms injection current at 600 pA in the IC pyramidal neurons from rats treated by Ado::CIW or Ado::CIE showed that, although no significant difference of the negative peak of AHPs between WD2 *vs*. WD21 (Fig. 3B, CIW/CIE × WD2/WD21 interaction $F_{1,59}$=0.1, p=0.81, cell-based; CIW/CIE × WD2/WD21 interaction $F_{1,15}$=0.03, p=0.86, animal-based), the after-fast AHP (fAHP) depolarization slope 0 to 8 sec after the AHP negative peak was significantly lower on WD21 than WD2 in rats treated by Ado::CIE (Fig. 3D, Time × WD2/WD21 interaction $F_{8,232}$=2.3, p=0.02, cell-based; Time × WD2/WD21 interaction $F_{8,56}$=2.1, p=0.048, animal-based) but not in those treated by

Ado::CIW (Fig. 3C, Time × WD2/WD21 interaction $F_{8,240}$=1.4, p=0.19, cell-based; Time × WD2/WD21 interaction $F_{8,64}$=1.5, p=0.18, animal-based). There were no differences in the after-fAHP depolarization slopes 0–8 sec after the AHP negative peak between Ado::CIW *vs.* Ado::CIE rats on either WD2 (Fig. 3E, Time × CIW/CIE interaction $F_{8,240}$=1.3, p=0.24, cell-based; Time × CIW/CIE interaction $F_{8,56}$=1.2, p=0.30, animal-based) or WD21 (Fig. 3F, Time × CIW/CIE interaction $F_{8,232}$=0.26, p=0.98, cell-based; Time × CIW/CIE interaction $F_{8,64}$=0.28, p=0.97, animal-based). Slower slope of after-fAHP depolarization in the Ado::CIE rats was accompanied by longer inter-spike intervals on WD21, relative to that on WD2 in the Ado::CIE rats or WD21 in the Ado::CIW rats (Fig. 3G, CIW/CIE × WD2/WD21 interaction $F_{1,59}$=10.0, p<0.01, cell-based; CIW/CIE × WD2/WD21 interaction $F_{1,15}$=7.9, p=0.01, animal-based). Nested t test on the amplitude 8 seconds after AHP negative peak in **D** showed more hyperpolarized on WD21, relative to that on WD2 after Ado::CIE (t_{29}=3.6, p<0.01). Further three-way ANOVA analyses on the AHP depolarization time course from both Ado::CIW and Ado::CIE on WD2 and WD21 (i.e., the data from both **C** and **D**, or from both **E** and **F**) showed no significant interactions of I_{inj} × WD2/WD21 × Ado::CIW/Ado::CIE ($F_{8,472}$=1.0, p=0.40), or WD2/WD21 × Ado::CIW/Ado::CIE ($F_{1,59}$=0.5, p=0.50). The amplitude of AHP peak was measured by the difference between action potential threshold and the negative peak of the hyperpolarized potential after the action potential, and the inter-spike interval was measured by the time difference between the onset of the 2nd to the 3rd spike (i.e., the location where the spike threshold was measured) induced by 300 ms of 600 pA injection current. Thus, the AHP amplitude, as well as the subsequent depolarization of the membrane potential by which the membrane potential returns to the RMP and allows further depolarization to initiate the next action potential, can be affected by the level of RMP and threshold of action potential, among other factors. It is important to note that no significant differences of RMPs (Fig. 3I, CIW/CIE × WD2/WD21 interaction $F_{1,59}$=0.08, p=0.78, cell-based; CIW/CIE × WD2/WD21 interaction $F_{1,15}$=0.03, p=0.86, animal-based) and the threshold of action potential (Fig. 3H, CIW/CIE × WD2/WD21 interaction $F_{1,59}$=2.9, p=0.09, cell-based; CIW/CIE × WD2/WD21 interaction $F_{1,15}$=3.0, p=0.10, animal-based) were observed. In addition, our recordings were done by adjusting the RMP to −70 ± 0.05 mV in order to exclude the variability of RMPs in individual neurons. Thus, we conclude there is a decrease in excitability of IC neurons in Ado::CIE by passage of the withdrawal period.

Decreased excitability 2 days but not 21 days after CIE during adult stage— Whole-cell patch clamp recordings of pyramidal neurons in the IC (example traces in Fig. 4A&B) were then performed on rats treated by CIW or CIE during their adult stage. A voltage-dependent decrease of spike numbers in the IC was observed on WD2 in rats treated by Adu::CIE, relative to Adu::CIW (Fig. 4E, I_{inj} × CIW/CIE interaction $F_{10,250}$=4.0, p<0.01, cell-based; I_{inj} × CIW/CIE interaction $F_{10,80}$=3.7, p<0.01, animal-based). However, no significant differences of spike number on WD 21 were detected on Adu::CIW *vs.* Adu::CIE rats (Fig. 4F, I_{inj} × CIW/CIE interaction $F_{10,450}$=1.1, p=0.40, cell-based; I_{inj} × CIW/CIE interaction $F_{10,120}$=1.3, p=0.24, animal-based). Interestingly, no differences of spike number on WD2 *vs.* WD21 were detected in rats treated by either Adu::CIW (Fig. 4C, I_{inj} × WD2/WD21 interaction $F_{10,360}$=1.4, p=0.18, cell-based; I_{inj} × WD2/WD21 interaction $F_{10,100}$=1.2, p=0.30, animal-based) or Adu::CIE (Fig. 4D, I_{inj} × WD2/WD21 interaction

$F_{10,340}$=0.3, p=0.99, cell-based; I_{inj} × WD2/WD21 interaction $F_{10,100}$=0.3, p=0.98, animal-based). Nested t test on the spike number at I_{inj}=600pA in **E** showed a significant decrease in Adu::CIE, relative to that in Adu::CIE (t_{25}=2.4, p=0.03). Further three-way ANOVA analyses on the spike number from both Adu::CIW and Adu::CIE on WD2 and WD21 (i.e., the data from both **C** and **D**, or from both **E** and **F**) showed no significant interactions of I_{inj} × WD2/WD21 × Ado::CIW/Ado::CIE ($F_{10,700}$=1.5, p=0.14), or WD2/WD21 × Adu::CIW/Adu::CIE ($F_{1,70}$=0.3, p=0.57). Thus, only a transient, but not prolonged, decrease of intrinsic excitability in the IC was observed in rats treated by Adu::CIE but not Adu::CIW.

Delayed after-fAHP depolarization 2 days after CIE during adult stage—We also analyzed the after-fAHP depolarization slope between 0 to 8 sec after the negative peak of AHPs collected in IC neurons 2 or 21 days after Adu::CIW or Adu::CIE treatment (example traces in Fig. 5A). Although no differences of AHP peak amplitude were detected between Adu::CIW *vs.* Adu::CIE on either WD2 or WD21 (Fig. 5B, CIW/CIE × WD2/WD21 interaction $F_{1,70}$=0.2, p=0.65, cell-based; CIW/CIE × WD2/WD21 interaction $F_{1,19}$=0.1, p=0.76, animal-based), decreased after-fAHP depolarization slope from the AHP negative peak was observed in Adu::CIE rats, relative to Adu::CIW, on WD2 (Fig. 5E, Time × CIW/CIE interaction $F_{8,200}$=16.2, p<0.01, cell-based; Time × CIW/CIE interaction $F_{8,64}$=14.1, p<0.01, animal-based), but not on WD21 (Fig. 5F, Time × CIW/CIE interaction $F_{8,360}$=1.7, p=0.10, cell-based; Time × CIW/CIE interaction $F_{8,96}$=1.5, p=0.17, animal-based). There were no differences in after-fAHP depolarization slope between WD2 *vs.* WD21 in rats treated by either Adu::CIW (Fig. 5C, Time × WD2/WD21 interaction $F_{8,288}$=1.1, p=0.35, cell-based; Time × WD2/WD21 interaction $F_{8,80}$=1.3, p=0.26, animal-based) or Adu::CIE (Fig. 5D, Time × WD2/WD21 interaction $F_{8,272}$=1.2, p=0.28, cell-based; Time × WD2/WD21 interaction $F_{8,80}$=1.2, p=0.29, animal-based). Nested t test on the amplitude 8 seconds after AHP negative peak in **E** showed more hyperpolarized on WD2 in Adu::CIE group, relative to that in Adu::CIE group (t_{29}=3.6, p<0.01). Further three-way ANOVA analyses on the AHP depolarization time course from both Ado::CIW and Ado::CIE on WD2 and WD21 (i.e., the data from both **C** and **D**, or from both **E** and **F**) showed significant interactions of I_{inj} × WD2/WD21 × Ado::CIW/Ado::CIE ($F_{8,560}$=2.0, p=0.04), and WD2/WD21 × Ado::CIW/Ado::CIE ($F_{8,560}$=9.0, p<0.01). Relative to WD2 in Adu::CIW rats, slower after-fAHP depolarization slope on WD2 in the Adu::CIE rats was accompanied by longer inter-spike intervals (Fig. 5G, CIW/CIE × WD2/WD21 interaction $F_{1,70}$=9.2, p<0.01, cell-based; CIW/CIE × WD2/WD21 interaction $F_{1,19}$=7.8, p=0.01, animal-based). Furthermore, the inter-spike interval (Fig. 5H, CIW/CIE × WD2/WD21 interaction $F_{1,70}$=0.01, p=0.94, cell-based; CIW/CIE × WD2/WD21 interaction $F_{1,19}$=0.01, p=0.92, animal-based) and RMP (Fig. 5I, CIW/CIE × WD2/WD21 interaction $F_{1,70}$=0.2, p=0.70, cell-based; CIW/CIE × WD2/WD21 interaction $F_{1,19}$=0.3, p=0.59, animal-based), as potential factors to affect after-fAHP depolarization slope, were not differentially influenced by Adu::CIE on either WD2 or WD21. Thus, the transiently decreased intrinsic excitability of IC neurons in Adu::CIE on WD2 can be specifically associated with reduced after-fAHP depolarization slope.

Similar effects of adolescent *vs*. adult CIE on I-V response and input resistance

Besides the specific effects of CIE treatment at different developmental (i.e., adolescent *vs*. adult) stages, CIE effects were also detected independent from the developmental stages. First, injection current-dependent depolarization of membrane voltage responses was observed with statistically significant difference on WD2 in both Ado::CIE, compared to Ado::CIW (Fig. 6C, I_{inj} × CIW/CIE interaction $F_{7,210}$=2.6, p=0.01, cell-based; I_{inj} × CIW/CIE interaction $F_{7,49}$=2.9, p=0.01, animal-based), and Adu::CIE, compared to Adu::CIW (Fig. 7C, I_{inj} × CIW/CIE interaction $F_{7,161}$=5.6, p<0.01, cell-based; I_{inj} × CIW/CIE interaction $F_{7,56}$=5.1, p<0.01, animal-based), but not on WD21 in Ado::CIE (Fig. 6D, I_{inj} × CIW/CIE interaction $F_{7,203}$=0.3, p=0.93, cell-based; I_{inj} × CIW/CIE interaction $F_{7,56}$=0.3, p=0.95, animal-based) or Adu::CIE (Fig. 7D, I_{inj} × CIW/CIE interaction $F_{7,287}$=1.1, p=0.34, cell-based; I_{inj} × CIW/CIE interaction $F_{7,84}$=1.0, p=0.45, animal-based). In addition, compared to WD2, the injection current-dependent depolarization of membrane voltage response was observed on WD21 in rats treated by both Ado::CIE (Fig. 6B, I_{inj} × WD2/WD21 interaction $F_{7,203}$=3.9, p<0.01, cell-based; I_{inj} × WD2/WD21 interaction $F_{7,49}$=3.1, p=0.01, animal-based) and Adu::CIE (Fig. 7B, I_{inj} × WD2/WD21 interaction $F_{7,196}$=6.0, p<0.01, cell-based; I_{inj} × WD2/WD21 interaction $F_{7,70}$=5.4, p<0.01, animal-based), but not in those treated by Ado::CIW (Fig. 6A, I_{inj} × WD2/WD21 interaction $F_{7,210}$=0.2, p=0.98, cell-based; I_{inj} × WD2/WD21 interaction $F_{7,56}$=0.4, p=0.90, animal-based) or Adu::CIW (Fig. 7A, I_{inj} × WD2/WD21 interaction $F_{7,252}$=0.7, p=0.67, cell-based; I_{inj} × WD2/WD21 interaction $F_{7,70}$=0.6, p=0.77, animal-based). Further three-way ANOVA analyses on the I-V response from both Ado::CIW and Ado::CIE on WD2 and WD21 (i.e., the data from both **6A** and **6B**, or from both **6C** and **6D**) showed significant interactions of I_{inj} × WD2/WD21 × Ado::CIW/Ado::CIE ($F_{7,413}$=2.3, p=0.02), although no interactions between WD2/WD21 × Ado::CIW/Ado::CIE ($F_{1,59}$=2.4, p=0.13). Three-way ANOVA analyses on the I-V response from both Adu::CIW and Adu::CIE on WD2 and WD21 (i.e., the data from both **7A** and **7B**, or from both **7C** and **7D**) showed significant interactions of I_{inj} × WD2/WD21 × Adu::CIW/Adu::CIE ($F_{7,441}$=4.9, p<0.01), although no interactions between WD2/WD21 × Adu::CIW/Ado::CIE ($F_{1,63}$=1.7, p=0.20).

Second, similar effects of CIE on input resistance, calculated by dividing the membrane voltage response by the injection current at −400 pA, were observed in rats receiving CIE during their adolescent and adult stages. Specifically, Ado:CIE rats on WD2 showed a smaller input resistance compared to either Ado::CIW on WD2 or Ado::CIE on WD21 (Fig. 8A, WD2/WD21 × CIW/CIE interaction $F_{1,59}$=5.4, p=0.02, cell-based; WD2/WD21 × CIW/CIE interaction $F_{1,15}$=4.9, p=0.043, animal-based). Adu::CIE rats on WD2 also showed a smaller input resistance compared to either Adu::CIW on WD2 or Adu::CIE on WD21 (Fig. 8B, WD2/WD21 × CIW/CIE interaction $F_{1,64}$=8.5, p<0.01, cell-based; WD2/WD21 × CIW/CIE interaction $F_{1,19}$=7.3, p=0.01, animal-based).

DISCUSSION

The involvement of the IC in alcohol-related behavioral output has been identified before. For example, excitatory projections from insular cortex to nucleus accumbens core integrates information about internal states by regulating aversion-resistant alcohol intake (Seif et

al., 2013). Silencing of the IC and its striatal projections can enhance sensitivity to the interoceptive effects of alcohol and decrease alcohol, but not sucrose, self-administration (Jaramillo, Randall, et al., 2018; Jaramillo, Van Voorhies, Randall, & Besheer, 2018). Although synaptic alterations induced by CIE have been extensively characterized in the IC as well as a variety of other brain regions, changes in intrinsic excitability of critical pyramidal neurons are understudied. Recent evidence suggests that prolonged alcohol drinking and alcohol dependence produce plasticity of intrinsic excitability as measured by changes in evoked action potential firing and AHP amplitude in the prefrontal and orbitofrontal cortices (Cannady, Rinker, Nimitvilai, Woodward, & Mulholland, 2018). Specifically, adolescent exposure to binge drinking is associated with specific changes in the intrinsic excitability of pyramidal neurons in the PFC, reducing the ability of these neurons to generate persistent intrinsic activity, a phenomenon thought to be important for working memory (Salling et al., 2018). However, little was known about the excitability changes in the IC.

Based on the present results, the effects of CIE are developmental stage of CIE exposure-dependent or independent. The adolescent stage is a critical period of brain maturation. Each brain region or each functional aspect of a certain brain region may have its own programmed maturation clock. Usually, the more mature a specific brain region or specific functional system, the lower the age-dependent vulnerability of the brain to the external insult (i.e., the CIE in this study). Three-way ANOVA analysis of the spike number evoked by I_{inj}=600pA from both adolescent CIW or CIE (Fig. 3) and adult CIW or CIE (Fig. 5) demonstrated significant interactions among the 3 factors, i.e., Ado vs. Adu, CIW vs. CIE, and WD2 vs. WD21 ($F_{1,129}$=4.1, p=0.04), supporting developmental stage-dependent changes in the intrinsic excitability. Together with the developmental stage-independent changes in the I-V response (Ado/Adu × CIW/CIE × WD2/WD21 interaction $F_{1,122}$<0.1, p=0.95, three-way ANOVA analysis at I_{inj}=−400pA in Figs. 6 and 7) and the membrane input resistance induced by CIE (Ado/Adu × CIW/CIE × WD2/WD21 interaction $F_{1,122}$=0.2, p=0.69, three-way ANOVA analysis at I_{inj}=−400pA in Figs. 8), we assume that the neuronal mechanisms involved in controlling the membrane input resistance are comparatively mature at the adolescent stage, while the neurobiological machinery system involved in intrinsic excitability is still not fully mature at this early developmental stage. It was interesting to notice that all the developmental stage-independent changes, including the I-V response curves and the membrane input resistance, are significant only on WD2 but not on WD21. This indicates that the developmental stage-independent changes are temporary, not prolonged. In sum, although changes were developmental stage-dependent, the decreased excitability was observed in rats after both Ado::CIE and Adu::CIE, consistent with the decreased activity in the IC reported by neuroimaging from human cases (Naqvi et al., 2007).

A potential factor that may affect IC excitability is the momentary stress produced by the IG administration. However, this procedure of oral solution delivery is well established in our laboratory and the experimental subjects do not appear to display negative reactions. In the absence of more a detailed evaluation of IC neuronal excitability from naïve controls, which received no IG administration, this concern could also be allayed by our experience with data from other brain regions, such as in the mPFC or the striatum where the slice

recordings were done but no significant effects were observed between naïve controls and water IG controls. It is also worth noting that the current studies were performed on male rats only. Sex differences have been reported in both human and laboratory animal studies suggesting differing baseline state of brain physiology or tonic functional activity between females and males (Macey et al., 2016; Wang, Guo, Mayer, & Holschneider, 2019). For example, substance abuse history increased and decreased the volume of IC in male and female human cases, respectively (Tanabe et al., 2013). Greater blood flow was detected in drug-using women, relative to drug-using men (Andersen, Sawyer, & Howell, 2012; Polak, Haug, Drachenberg, & Svikis, 2015). Also, the female reproductive cycle (i.e., proestrus, estrus, metestrus, and diestrus) could be a significant factor leading to cycle stage-specific behavioral variability and neuronal alterations as a response to the CIE treatment (Galaj, Kipp, Floresco, & Savage, 2019; Li et al., 2019; Marco et al., 2017; Yttri, Burk, & Hunt, 2004).

Withdrawal is a key factor for the age-dependent effects of CIE on neuronal excitability. Our data showed that the effects of CIE on intrinsic excitability in adult brains are reversible. However, the effects of adolescent CIE could be permanent as a consequence of significant alterations during the prolonged withdrawal period. This may explain the vulnerability of adolescent brains to the neuronal deleterious effects of binge alcohol exposure. Unlike adult binge alcohol exposure, which is followed by significant early withdrawal effects in the AAI, the adolescent binge alcohol exposure showed no early withdrawal effects on the intrinsic excitability of the AAI projecting neurons. This is similar to clinical documentation in which the prolonged effects of binge drinking are more frequently observed in those who start during their adolescence (Molina & Nelson, 2018). No obvious changes of excitability in the AAI were observed right after adolescent CIE treatment. We assume that the transient effects of Ado::CIE may be encoded in the AAI in a more subtle manner or by different signaling pathways. Further, acute effects of Ado::CIE in other brain regions cannot be excluded, which also could modify their intrinsic excitability gradually during the passage of withdrawal period. It is suggested that the AAI could be a target at the later withdrawal stage from adolescent binge alcohol exposure. Further explorations of the neuronal substrates inside or outside the AAI are needed.

The effects of CIE, including both Ado::CIE and Adu::CIE, were detected only at relatively high intracellular current injections. For example, only significance of Bonferroni post-hoc test on the spike number was observed by injecting currents as high as 600 pA. In addition, only significance of Bonferroni post-hoc test on I-V curve was detected with an injection current at −300 pA or more negative. Finally, significant interactions between CIW/CIE and WD2/WD21 were detected by 2-way ANOVA on the membrane input resistance calculated by the change of membrane voltage induced by −400 pA. Although alterations became evident only at highly depolarized or hyperpolarized membrane potentials, we believe that the effects of CIE are not outside the physiological range, as supported by the following facts. Recordings *in vitro* are flawed due to low K^+ concentration in the ACSF and the sparsity of excitatory inputs compared to more physiological conditions, i.e., *in vivo*. This limitation of slice recordings leads to artificially hyperpolarized RMP and reduced excitability, but allows more precise measurements of firing frequency and action potential properties less amenable during *in vivo* conditions. In our experiments we held

the membrane at −70mV and from there we stimulated at various intensities to construct input-output relationships. Even at the highest depolarizing current intensities, the firing frequency was never beyond 40 Hz, well within a physiological range when compared to *in vivo* situation where pyramidal neurons can fire at higher frequencies, probably as high as 55 Hz (Kawaguchi, 2001). Another proof that our recording conditions were not unusual, is the fact that we did not observe depolarization block of action potential firing or abnormal rectification at highly hyperpolarized membrane potentials.

Generally speaking, the excitability of pyramidal neurons can be affected by, among others, the membrane input resistance and the amplitude of the action potential AHP (Mu et al., 2010), including both the medium AHP (mAHP), assumed to be mediated by small conductance (SK) calcium-activated potassium channels, and the fast AHP (fAHP), assumed to be mediated by large conductance (BK) calcium-activated potassium channels (Ishikawa et al., 2009). Both SK and BK channels have been studied, although in other brain regions such as nucleus accumbens, in rodents treated by CIE. Manipulation of BK or SK potassium channels can adjust the anxiety level, alcohol drinking behaviors, *etc.* (Kreifeldt, Le, Treistman, Koob, & Contet, 2013; Shan et al., 2019). As we mentioned, the difference of intrinsic excitability between CIW *vs.* CIE was significantly detected with high positive injection current (e.g., +600 pA), but not at the low positive injection currents. This led to difficulties in identifying the BK *vs.* SK channel because of the short interval between spikes at high positive injection currents (i.e., usually <10 ms when I_{inj}=600pA). After finding no significant differences of the peak AHP, which is assumed to be mediated by BK channel, rather than measuring the mAHP, which is assumed to be mediated by SK channel and usually detected >=10 ms after the onset of the action potential) (Shan et al., 2019), the AHP amplitude in the following 8 seconds was measured and a delayed recovery during the first 8 seconds after fAHP was accompanied with decreased excitability. The channel mechanisms of the early after-fAHP depolarization right after fAHP needs to be explored in the future by applying both channel blockers/activators of SK and BK channels.

The current study is just an example of how to refine our molecular and cellular explorations in the IC of subjects with a history of adolescent binge alcohol. There are many ways to further refine this research direction before detailed neuronal mechanisms of the IC can be found in mediating the acute and prolonged behavioral consequences after adolescent binge alcohol drinking. ***First***, besides the AAI, future studies may be designed in other IC subregions, including the granular insular, which has been evidenced as a novel brain region to prevent nicotine addiction, and the dysgranular insula as the intermediate relay between the rostral agranular and caudal granular IC but rarely investigated in alcohol research (Forget, Pushparaj, & Le Foll, 2010). ***Second***, within the AAI, a further refined study may be performed by isolating the dorsal and ventral AAI, which was not carefully identified in the current study, although most of our recordings were done in the dorsal compartment of the AAI. The ventral AAI is exclusively innervated by olfactory areas of the limbic system (such as primary olfactory cortex, posterolateral amygdala, and lateral entorhinal cortex) while dorsal AAI receives major afferent projections from non-olfactory limbic areas (lateral and basolateral amygdala as an example)(Reep & Winans, 1982). ***Third***, other types of

neurons, such as GABAergic or cholinergic interneurons, in the AAI should be explored in animal models with a history of Ado::CIE.

Acknowledgments

SUPPORT OR GRANT INFORMATION

This work was supported by NIH grants (R01AA025784, P50AA017823, T32AA025606) and Brain & Behavior Research Foundation grant #24989.

Data Availability Statement

The data that support the findings of this study are available from the corresponding author upon reasonable request.

REFERENCES

Abernathy K, Chandler LJ, & Woodward JJ (2010). Alcohol and the prefrontal cortex. Int Rev Neurobiol, 91, 289–320. doi:10.1016/S0074-7742(10)91009-X [PubMed: 20813246]

Allen GV, Saper CB, Hurley KM, & Cechetto DF (1991). Organization of visceral and limbic connections in the insular cortex of the rat. J Comp Neurol, 311(1), 1–16. doi:10.1002/cne.903110102 [PubMed: 1719041]

Andersen ML, Sawyer EK, & Howell LL (2012). Contributions of neuroimaging to understanding sex differences in cocaine abuse. Exp Clin Psychopharmacol, 20(1), 2–15. doi:10.1037/a0025219 [PubMed: 21875225]

Baumgartner U, Buchholz HG, Bellosevich A, Magerl W, Siessmeier T, Rolke R, … Schreckenberger M (2006). High opiate receptor binding potential in the human lateral pain system. Neuroimage, 30(3), 692–699. doi:10.1016/j.neuroimage.2005.10.033 [PubMed: 16337817]

Burkey AR, Carstens E, Wenniger JJ, Tang J, & Jasmin L (1996). An opioidergic cortical antinociception triggering site in the agranular insular cortex of the rat that contributes to morphine antinociception. J Neurosci, 16(20), 6612–6623. [PubMed: 8815937]

Cannady R, Rinker JA, Nimitvilai S, Woodward JJ, & Mulholland PJ (2018). Chronic Alcohol, Intrinsic Excitability, and Potassium Channels: Neuroadaptations and Drinking Behavior. Handb Exp Pharmacol, 248, 311–343. doi:10.1007/164_2017_90 [PubMed: 29374839]

Contreras M, Ceric F, & Torrealba F (2007). Inactivation of the interoceptive insula disrupts drug craving and malaise induced by lithium. Science, 318(5850), 655–658. doi:10.1126/science.1145590 [PubMed: 17962567]

Damasio AR, Grabowski TJ, Bechara A, Damasio H, Ponto LL, Parvizi J, & Hichwa RD (2000). Subcortical and cortical brain activity during the feeling of self-generated emotions. Nat Neurosci, 3(10), 1049–1056. doi:10.1038/79871 [PubMed: 11017179]

Evans JM, Bey V, Burkey AR, & Commons KG (2007). Organization of endogenous opioids in the rostral agranular insular cortex of the rat. J Comp Neurol, 500(3), 530–541. doi:10.1002/cne.21197 [PubMed: 17120290]

Forget B, Pushparaj A, & Le Foll B (2010). Granular insular cortex inactivation as a novel therapeutic strategy for nicotine addiction. Biol Psychiatry, 68(3), 265–271. doi:10.1016/j.biopsych.2010.01.029 [PubMed: 20299008]

Franklin TR, Acton PD, Maldjian JA, Gray JD, Croft JR, Dackis CA, … Childress AR. (2002). Decreased gray matter concentration in the insular, orbitofrontal, cingulate, and temporal cortices of cocaine patients. Biol Psychiatry, 51(2), 134–142. [PubMed: 11822992]

Galaj E, Kipp BT, Floresco SB, & Savage LM (2019). Persistent Alterations of Accumbal Cholinergic Interneurons and Cognitive Dysfunction after Adolescent Intermittent Ethanol Exposure. Neuroscience, 404, 153–164. doi:10.1016/j.neuroscience.2019.01.062 [PubMed: 30742967]

Gaspar P, Berger B, Febvret A, Vigny A, & Henry JP (1989). Catecholamine innervation of the human cerebral cortex as revealed by comparative immunohistochemistry of tyrosine hydroxylase

and dopamine-beta-hydroxylase. J Comp Neurol, 279(2), 249–271. doi:10.1002/cne.902790208 [PubMed: 2563268]

Gogolla N (2017). The insular cortex. Curr Biol, 27(12), R580–R586. doi:10.1016/j.cub.2017.05.010 [PubMed: 28633023]

Hille B (2001). Ion channels of excitable membranes. 507.

Honrath B, Krabbendam IE, Culmsee C, & Dolga AM (2017). Small conductance Ca(2+)-activated K(+) channels in the plasma membrane, mitochondria and the ER: Pharmacology and implications in neuronal diseases. Neurochem Int, 109, 13–23. doi:10.1016/j.neuint.2017.05.005 [PubMed: 28511953]

Hurd YL, Suzuki M, & Sedvall GC (2001). D1 and D2 dopamine receptor mRNA expression in whole hemisphere sections of the human brain. J Chem Neuroanat, 22(1–2), 127–137. [PubMed: 11470560]

Ishikawa M, Mu P, Moyer JT, Wolf JA, Quock RM, Davies NM, … Dong Y. (2009). Homeostatic synapse-driven membrane plasticity in nucleus accumbens neurons. J Neurosci, 29(18), 5820–5831. doi:10.1523/JNEUROSCI.5703-08.2009 [PubMed: 19420249]

Jaramillo AA, Randall PA, Stewart S, Fortino B, Van Voorhies K, & Besheer J (2018). Functional role for cortical-striatal circuitry in modulating alcohol self-administration. Neuropharmacology, 130, 42–53. doi:10.1016/j.neuropharm.2017.11.035 [PubMed: 29183687]

Jaramillo AA, Van Voorhies K, Randall PA, & Besheer J (2018). Silencing the insular-striatal circuit decreases alcohol self-administration and increases sensitivity to alcohol. Behav Brain Res, 348, 74–81. doi:10.1016/j.bbr.2018.04.007 [PubMed: 29660441]

Kawaguchi Y (2001). Distinct firing patterns of neuronal subtypes in cortical synchronized activities. J Neurosci, 21(18), 7261–7272. [PubMed: 11549736]

Klenowski PM (2018). Emerging role for the medial prefrontal cortex in alcohol-seeking behaviors. Addict Behav, 77, 102–106. doi:10.1016/j.addbeh.2017.09.024 [PubMed: 28992574]

Kreifeldt M, Le D, Treistman SN, Koob GF, & Contet C (2013). BK channel beta1 and beta4 auxiliary subunits exert opposite influences on escalated ethanol drinking in dependent mice. Front Integr Neurosci, 7, 105. doi:10.3389/fnint.2013.00105 [PubMed: 24416005]

Kyzar EJ, Zhang H, & Pandey SC (2019). Adolescent Alcohol Exposure Epigenetically Suppresses Amygdala Arc Enhancer RNA Expression to Confer Adult Anxiety Susceptibility. Biol Psychiatry, 85(11), 904–914. doi:10.1016/j.biopsych.2018.12.021 [PubMed: 30827484]

Li J, Chen P, Han X, Zuo W, Mei Q, Bian EY, … Ye J. (2019). Differences between male and female rats in alcohol drinking, negative affects and neuronal activity after acute and prolonged abstinence. Int J Physiol Pathophysiol Pharmacol, 11(4), 163–176. [PubMed: 31523363]

Ma YY, Cepeda C, Chatta P, Franklin L, Evans CJ, & Levine MS (2012). Regional and cell-type-specific effects of DAMGO on striatal D1 and D2 dopamine receptor-expressing medium-sized spiny neurons. ASN Neuro, 4(2). doi:10.1042/an20110063

Ma YY, Lee BR, Wang X, Guo C, Liu L, Cui R, … Dong Y. (2014). Bidirectional modulation of incubation of cocaine craving by silent synapse-based remodeling of prefrontal cortex to accumbens projections. Neuron, 83(6), 1453–1467. doi:10.1016/j.neuron.2014.08.023 [PubMed: 25199705]

Ma YY, Wang X, Huang Y, Marie H, Nestler EJ, Schluter OM, & Dong Y (2016). Re-silencing of silent synapses unmasks anti-relapse effects of environmental enrichment. Proc Natl Acad Sci U S A, 113(18), 5089–5094. doi:10.1073/pnas.1524739113 [PubMed: 27091967]

Macey PM, Rieken NS, Kumar R, Ogren JA, Middlekauff HR, Wu P, … Harper RM. (2016). Sex Differences in Insular Cortex Gyri Responses to the Valsalva Maneuver. Front Neurol, 7, 87. doi:10.3389/fneur.2016.00087 [PubMed: 27375549]

Mackey S, & Paulus M (2013). Are there volumetric brain differences associated with the use of cocaine and amphetamine-type stimulants? Neurosci Biobehav Rev, 37(3), 300–316. doi:10.1016/j.neubiorev.2012.12.003 [PubMed: 23253945]

Marco EM, Penasco S, Hernandez MD, Gil A, Borcel E, Moya M, … Rodriguez de Fonseca F. (2017). Long-Term Effects of Intermittent Adolescent Alcohol Exposure in Male and Female Rats. Front Behav Neurosci, 11, 233. doi:10.3389/fnbeh.2017.00233 [PubMed: 29234279]

Molina PE, & Nelson S (2018). Binge Drinking's Effects on the Body. Alcohol Res, 39(1), 99–109. [PubMed: 30557153]

Mu P, Moyer JT, Ishikawa M, Zhang Y, Panksepp J, Sorg BA, … Dong Y. (2010). Exposure to cocaine dynamically regulates the intrinsic membrane excitability of nucleus accumbens neurons. J Neurosci, 30(10), 3689–3699. doi:10.1523/JNEUROSCI.4063-09.2010 [PubMed: 20220002]

Naqvi NH, Rudrauf D, Damasio H, & Bechara A (2007). Damage to the insula disrupts addiction to cigarette smoking. Science, 315(5811), 531–534. doi:10.1126/science.1135926 [PubMed: 17255515]

National Institute on Alcohol Abuse and Alcoholism, N. (2017). Underage Drinking.

Park SQ, Kahnt T, Beck A, Cohen MX, Dolan RJ, Wrase J, & Heinz A (2010). Prefrontal cortex fails to learn from reward prediction errors in alcohol dependence. J Neurosci, 30(22), 7749–7753. doi:10.1523/JNEUROSCI.5587-09.2010 [PubMed: 20519550]

Polak K, Haug NA, Drachenberg HE, & Svikis DS (2015). Gender Considerations in Addiction: Implications for Treatment. Curr Treat Options Psychiatry, 2(3), 326–338. doi:10.1007/s40501-015-0054-5 [PubMed: 26413454]

Reep RL, & Winans SS (1982). Afferent connections of dorsal and ventral agranular insular cortex in the hamster Mesocricetus auratus. Neuroscience, 7(5), 1265–1288. [PubMed: 7110587]

Sakharkar AJ, Kyzar EJ, Gavin DP, Zhang H, Chen Y, Krishnan HR, … Pandey SC. (2019). Altered amygdala DNA methylation mechanisms after adolescent alcohol exposure contributes to adult anxiety and alcohol drinking. Neuropharmacology, 107679. doi:10.1016/j.neuropharm.2019.107679 [PubMed: 31229451]

Salling MC, Skelly MJ, Avegno E, Regan S, Zeric T, Nichols E, & Harrison NL (2018). Alcohol Consumption during Adolescence in a Mouse Model of Binge Drinking Alters the Intrinsic Excitability and Function of the Prefrontal Cortex through a Reduction in the Hyperpolarization-Activated Cation Current. J Neurosci, 38(27), 6207–6222. doi:10.1523/jneurosci.0550-18.2018 [PubMed: 29915134]

Seif T, Chang SJ, Simms JA, Gibb SL, Dadgar J, Chen BT, … Hopf FW. (2013). Cortical activation of accumbens hyperpolarization-active NMDARs mediates aversion-resistant alcohol intake. Nat Neurosci, 16(8), 1094–1100. doi:10.1038/nn.3445 [PubMed: 23817545]

Shan L, Galaj E, & Ma YY (2019). Nucleus accumbens shell small conductance potassium channels underlie adolescent ethanol exposure-induced anxiety. Neuropsychopharmacology. doi:10.1038/s41386-019-0415-7

Shillinglaw JE, Morrisett RA, & Mangieri RA (2018). Ethanol Modulates Glutamatergic Transmission and NMDAR-Mediated Synaptic Plasticity in the Agranular Insular Cortex. Front Pharmacol, 9, 1458. doi:10.3389/fphar.2018.01458 [PubMed: 30618752]

Spear LP, & Swartzwelder HS (2014). Adolescent alcohol exposure and persistence of adolescent-typical phenotypes into adulthood: a mini-review. Neurosci Biobehav Rev, 45, 1–8. doi:10.1016/j.neubiorev.2014.04.012 [PubMed: 24813805]

Stewart JL, Connolly CG, May AC, Tapert SF, Wittmann M, & Paulus MP (2014). Striatum and insula dysfunction during reinforcement learning differentiates abstinent and relapsed methamphetamine-dependent individuals. Addiction, 109(3), 460–471. doi:10.1111/add.12403 [PubMed: 24329936]

Stewart JL, May AC, Poppa T, Davenport PW, Tapert SF, & Paulus MP (2014). You are the danger: attenuated insula response in methamphetamine users during aversive interoceptive decision-making. Drug Alcohol Depend, 142, 110–119. doi:10.1016/j.drugalcdep.2014.06.003 [PubMed: 24993186]

Substance Abuse and Mental Health Services Administration, S. (2015). Key Substance Use and Mental Health Indicators in the United States: Results from the 2015. National Survey on Drug Use and Health.

Suhara T, Yasuno F, Sudo Y, Yamamoto M, Inoue M, Okubo Y, & Suzuki K (2001). Dopamine D2 receptors in the insular cortex and the personality trait of novelty seeking. Neuroimage, 13(5), 891–895. doi:10.1006/nimg.2001.0761 [PubMed: 11304084]

Tanabe J, York P, Krmpotich T, Miller D, Dalwani M, Sakai JT, … Rojas DC. (2013). Insula and orbitofrontal cortical morphology in substance dependence is modulated by sex. AJNR Am J Neuroradiol, 34(6), 1150–1156. doi:10.3174/ajnr.A3347 [PubMed: 23153869]

Teofilovski G (1984). Anatomic characteristics of the grivet monkey insula. Acta Med Iugosl, 38(4), 241–246. [PubMed: 6507140]

Trantham-Davidson H, Burnett EJ, Gass JT, Lopez MF, Mulholland PJ, Centanni SW, … Chandler LJ (2014). Chronic alcohol disrupts dopamine receptor activity and the cognitive function of the medial prefrontal cortex. J Neurosci, 34(10), 3706–3718. doi:10.1523/JNEUROSCI.0623-13.2014 [PubMed: 24599469]

Uddin LQ, Nomi JS, Hebert-Seropian B, Ghaziri J, & Boucher O (2017). Structure and Function of the Human Insula. J Clin Neurophysiol, 34(4), 300–306. doi:10.1097/WNP.0000000000000377 [PubMed: 28644199]

Viner RM, & Taylor B (2007). Adult outcomes of binge drinking in adolescence: findings from a UK national birth cohort. J Epidemiol Community Health, 61(10), 902–907. doi:10.1136/jech.2005.038117 [PubMed: 17873228]

Wang Z, Guo Y, Mayer EA, & Holschneider DP (2019). Sex differences in insular functional connectivity in response to noxious visceral stimulation in rats. Brain Res, 1717, 15–26. doi:10.1016/j.brainres.2019.04.005 [PubMed: 30974090]

Yttri EA, Burk JA, & Hunt PS (2004). Intermittent ethanol exposure in adolescent rats: dose-dependent impairments in trace conditioning. Alcohol Clin Exp Res, 28(10), 1433–1436. doi:10.1097/01.alc.0000147657.51745.a7 [PubMed: 15597074]

SIGNIFICANCE STATEMENT

Alcohol is the most widely abused substance, particularly among adolescents. The internal mental state, primarily regulated by the insular cortex, is significantly and permanently affected by adolescent binge alcohol exposure, but we know little about the associated neuronal mechanisms. The present study showed significant alterations of pyramidal neurons in the IC during the prolonged withdrawal period after chronic intermittent ethanol exposure in the adolescent but not adult stage. This newly identified neuronal substrate may be targeted to treat those with adolescent binge history in order to prevent its prolonged mental effects.

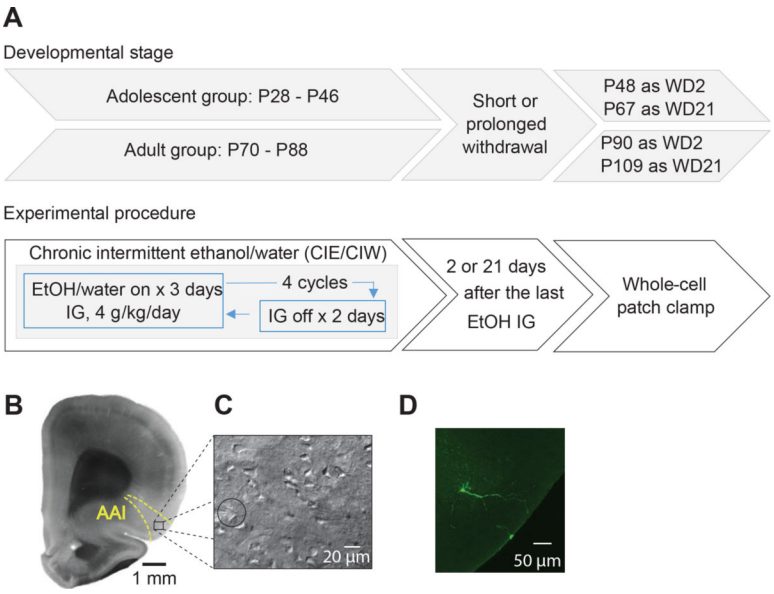

Figure 1. Experimental timeline and the whole-cell patch clamp recordings in the AAI

A, Experimental timeline. **B**, Example DIC image of coronal section at a low magnification (through 4X objective) showing the anatomical boundaries used to collect data from the AAI. **C**, Example DIC image of coronal section at a high magnification (through 40X objective) showing the whole-cell patch clamp recordings of pyramidal neurons in the IC. **D**, Example confocal images of pyramidal neuron in the AAI of an adult rat.

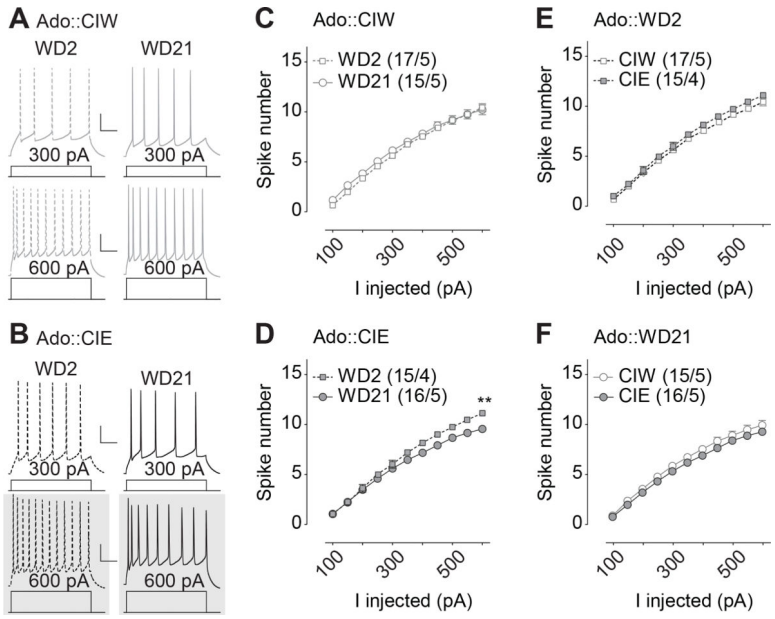

Figure 2. Decreased excitability 21 days but not 2 days after CIE during adolescent stage

A, B, Example traces showing action potentials elicited by 300 and 600 pA current injections in current clamp mode from rats treated with CIW (**A**) and CIE (**B**) during the adolescent stage. **C**,**D**, Summarized data showing that, although there is no injected current-dependent difference in excitability of the AAI pyramidal neurons between WD2 *vs.* WD21 from rats treated with Ado::CIW (**C**), a significant difference of spike number between WD2 *vs.* WD21 was observed in Ado::CIE rats (**D**). **E**,**F**, Summarized data showing no injected current-dependent difference in excitability of the AAI pyramidal neurons between Ado::CIW *vs.* Ado::CIE on WD2 (**E**) or WD21 (**F**). Except in cases with other statistics as specified in the RESULTS, data were analyzed by two-way ANOVA with repeated measures (**C-F**), followed by Bonferroni post-hoc tests. n/m, the number of cells/animals for data collection. *, $p<0.05$. Gray shadow in **A** and **B**, example traces presenting the statistical difference. Scale bars, 60 ms and 20 mV.

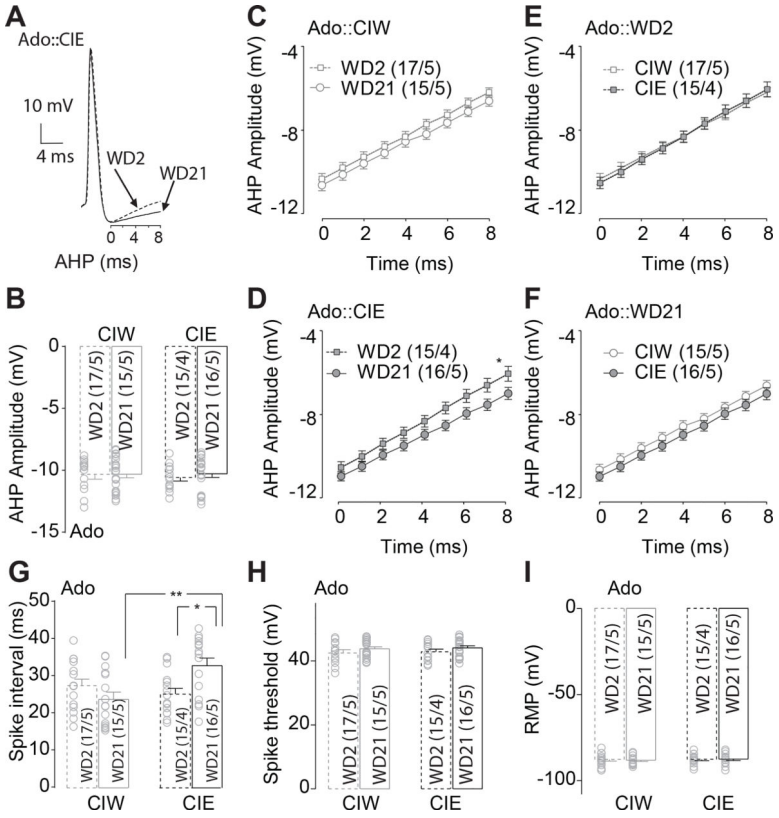

Figure 3. Delayed depolarization of AHP 21 days after adolescent CIE treatment

A, Example traces showing the delayed depolarization of the AHP during the first 8 second after the negative peak of AHP. **B**, Summarized data showing no significant effects of Ado::CIE on the negative peak of AHP. **C**, **D**, Summarized data showing that, although no significant difference of the AHP depolarization during the first 8 seconds after the negative peak of the AHP in Ado::CIW (**C**), a delayed depolarization of the AHP was observed on WD21, compared to that on WD2, in Ado::CIE rats (**D**). **E**, **F**, Summarized data showing no significant difference of the AHP depolarization during the first 8 seconds after the negative peak of the AHP in rats treated by Ado::CIW *vs.* Ado::CIE on either WD2 (**E**) or WD21 (**F**). **G**, Summarized data showing significant longer spike-intervals in rats treated by Ado::CIE on WD21. **H**, Summarized data showing no significant effects of Adu::CIE on the action potential threshold. **I**, Summarized data showing no significant effects of Adu::CIE on the RMP. Except in cases with other statistics as specified in the RESULTS, data were analyzed by two-way ANOVA (**B**, **G-I**) or two-way ANOVA with repeated measures (**C-F**), followed by Bonferroni post-hoc tests. n/m, the number of cells/animals for data collection. *, $p<0.05$.

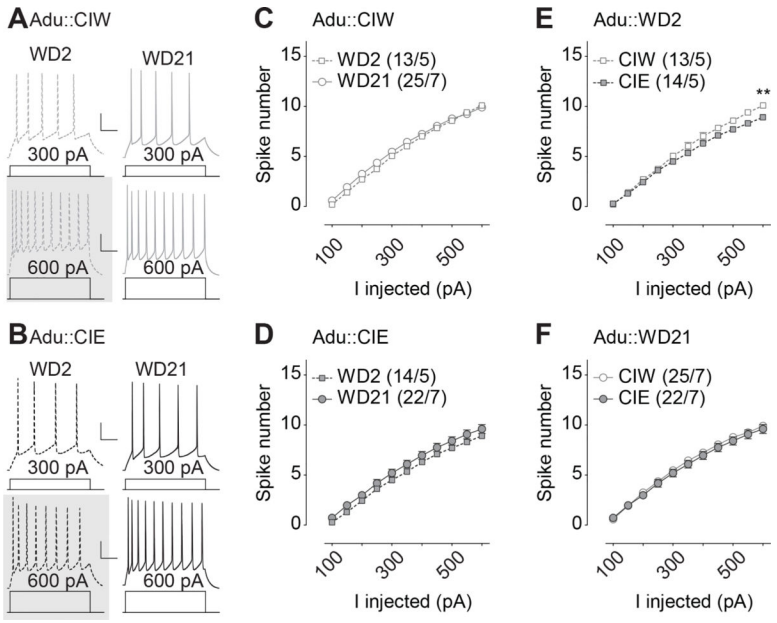

Figure 4. Insular excitability 2 days and 21 days after CIE during adult stage

A, B, Example traces showing action potentials elicited by 300 and 600 pA current injections in current clamp mode from rats treated with CIW (**A**) and CIE (**B**) during the adult stage. **C**,**D**, Summarized data showing no injected current-dependent difference in excitability of the AAI pyramidal neurons between WD2 *vs.* WD21 from rats treated with Adu::CIW (**C**) or Adu::CIE (**D**). **E**,**F**, Summarized data showing significant injected current-dependent differences in excitability of the AAI pyramidal neurons between Adu::CIW *vs.* Adu::CIE on WD2 (**E**) but not on WD21 (**F**). Except in cases with other statistics as specified in the RESULTS, data were analyzed by two-way ANOVA with repeated measures (**C**-**F**), followed by Bonferroni post-hoc tests. n/m, the number of cells/animals for data collection. **, $p<0.01$. Gray shadow in **A** and **B**, example traces presenting the statistical difference.

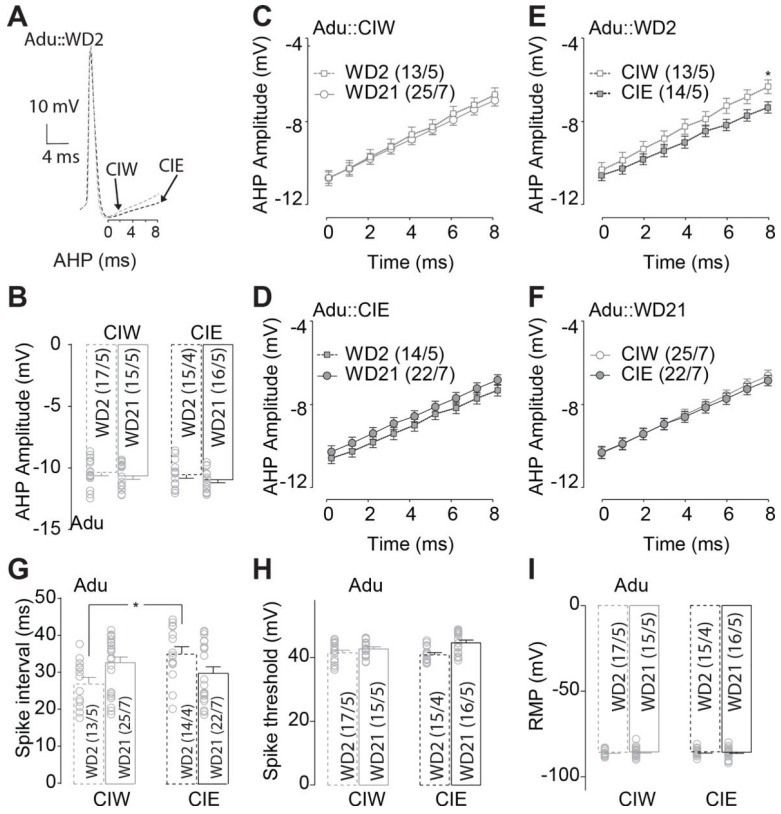

Figure 5. Delayed depolarization of AHP 2 days after CIE during adult stage

A, Example traces showing the delayed depolarization of the AHP during the first 8 second after the negative peak of AHP. **B**, Summarized data showing no significant effects of Adu::CIE on the negative peak of AHP. **C**, **D**, Summarized data showing no significant difference of the AHP depolarization during the first 8 seconds after the negative peak of the AHP in Adu::CIW (**C**) or Adu::CIE treated rats (**D**). **E**, **F**, Summarized data showing, significant differences of the AHP depolarization during the first 8 seconds after the negative peak of the AHP between Adu::CIW vs. Adu::CIE on WD2 (**E**) but not WD21 (**F**). **G**, Summarized data showing significant longer spike-intervals in rats treated by Adu::CIE on WD2. **H**, Summarized data showing no significant effects of Adu::CIE on the action potential threshold. **I**, Summarized data showing no significant effects of Adu::CIE on the RMP. Except in cases with other statistics as specified in the RESULTS, data were analyzed by two-way ANOVA (**B, G-I**) or two-way ANOVA with repeated measures (**C-F**), followed by Bonferroni post-hoc tests. n/m, the number of cells/animals for data collection. *, $p<0.05$.

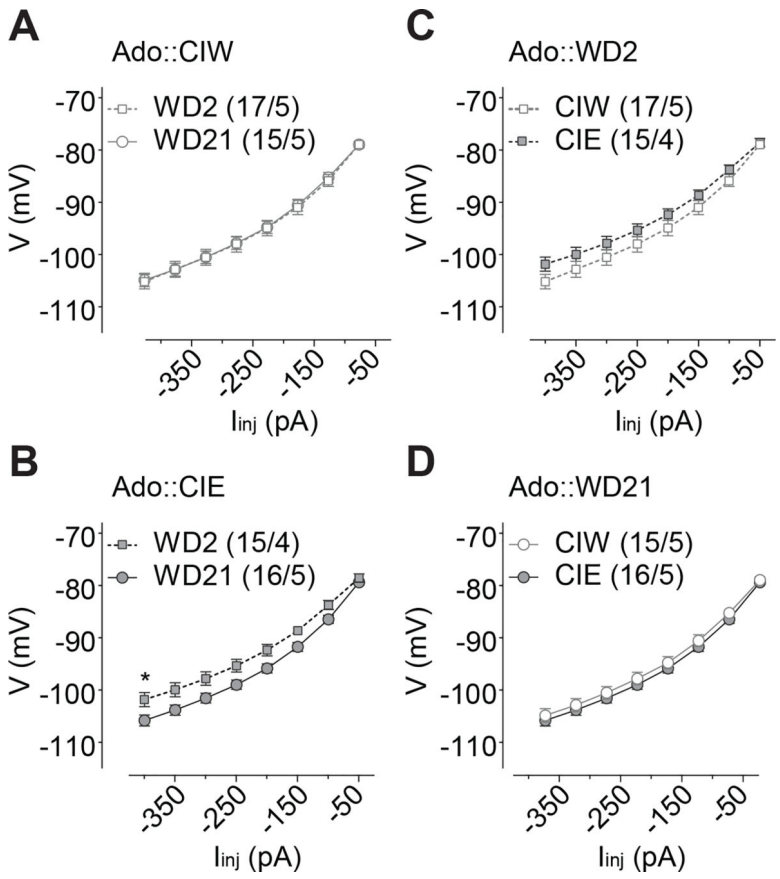

Figure 6. Injection current-dependent differences of the membrane change observed on WD2 in rats with a history of Ado::CIE

A, **B**, Summarized data showing that, although no significant difference of the I-V input-out response curves between WD2 *vs.* WD21 in Ado::CIW rats (**A**), significantly different I-V input-output response curves between WD2 *vs.* WD21 were observed in Ado::CIE rats (**B**). **C**, **D**, Summarized data showing significant differences of the I-V input-out response curves between in rats treated by Ado::CIW *vs.* Ado::CIE on WD2 (**C**) but not WD21 (**D**). Except in cases with other statistics as specified in the RESULTS, data were analyzed by two-way ANOVA with repeated measures, followed by Bonferroni post-hoc tests. n/m, the number of cells/animals for data collection. *, $p<0.05$.

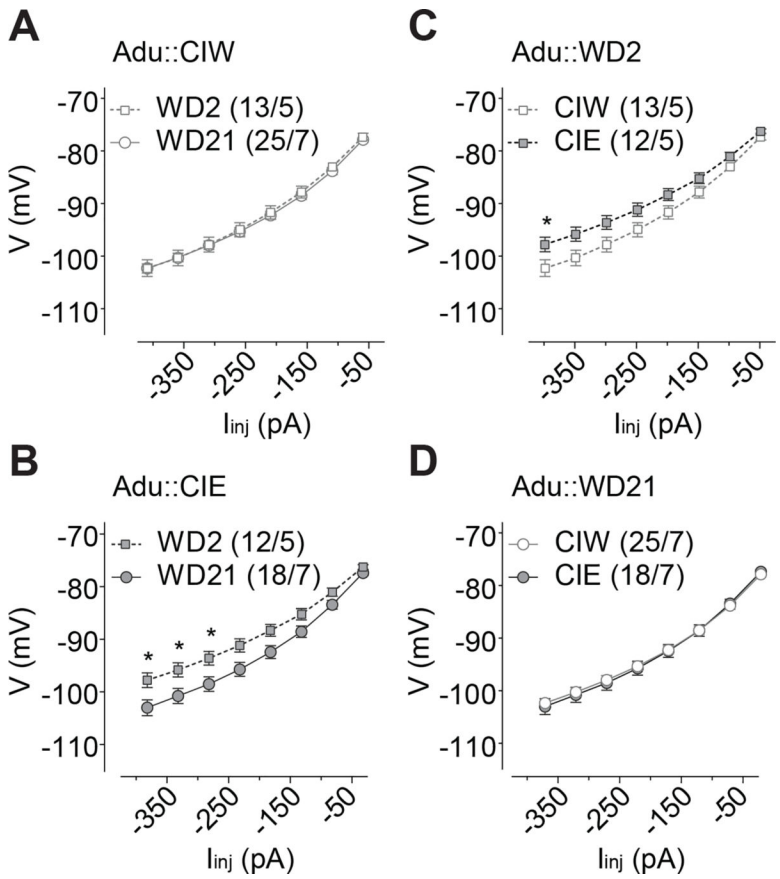

Figure 7. Injection current-dependent differences of the membrane change observed on WD2 in rats with a history of Adu::CIE

A, **B**, Summarized data showing that, although no significant difference of the I-V input-out response curves between WD2 *vs.* WD21 in Adu::CIW rats (**A**), significantly different I-V input-out response curves between WD2 *vs.* WD21 were observed in Adu::CIE rats (**B**). **C**, **D**, Summarized data showing significant differences of the I-V input-out response curves in rats treated by Adu::CIW *vs.* Adu::CIE on WD2 (**C**) but not WD21 (**D**). Except in cases with other statistics as specified in the RESULTS, data were analyzed by two-way ANOVA with repeated measures, followed by Bonferroni post-hoc tests. n/m, the number of cells/animals for data collection. *, $p<0.05$.

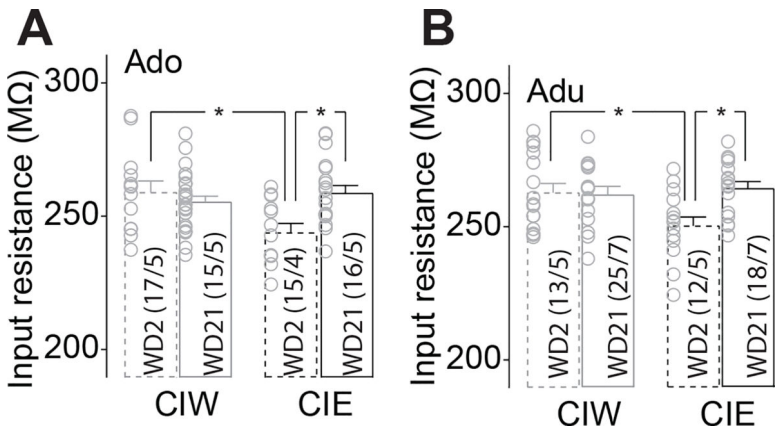

Figure 8. lower membrane input resistance was observed on WD 2 in rats with a history of Adu::CIE or Adu::CIE

A, Summarized data showing withdrawal-stage dependent effects of Ado::CIE on input resistance. **B**, Summarized data showing withdrawal-stage dependent effects of Adu::CIE on input resistance. Except in cases with other statistics as specified in the RESULTS, data were analyzed by two-way ANOVA, followed by Bonferroni post-hoc tests. n/m, the number of cells/animals for data collection. *, $p<0.05$.